

# LOW IMPEDANCE DESIGN WITH EXAMPLE OF KICKERS (INCLUDING CABLES) AND POTENTIAL OF METAMATERIALS

C. Zannini\*, M. Barnes, N. Biancacci, A. Danisi, E. Koukovini-Platia, E. Métral, G. Rumolo, B. Salvant,  
CERN, 1211 Geneva, Switzerland

## Abstract

Unmatched terminations of single elements were recently identified to be responsible for beam instabilities in the CERN PSB and LEIR machines. Impedance models are needed to estimate the impedance of similar devices and to assess potential intensity limitations. A circuitual model that includes the effect of coupling to cables on the beam coupling impedance will be discussed. Moreover, examples of low impedance design with special emphasis on the mitigation of the impedance of ferrite kickers (e.g. longitudinal serigraphy) will be presented and guidelines for optimized impedance design will be provided. Finally, the potential of metamaterials for impedance mitigation will be discussed.

## INTRODUCTION

A correct modeling of the beam coupling impedance of accelerator elements is essential to identify potential issues and to build an accurate impedance model of the complete accelerator for beam dynamics studies. The beam coupling impedance can cause issues on single accelerator elements (equipment degradation and damage due to induced heating or sparking) as well as instability of the particle beam. Both the undesired effects translate into intensity limitations. Therefore, the optimization of the beam coupling impedance is crucial to push the performance of the accelerators and to achieve the desired beam. In order to optimize the design of accelerator elements, firstly the consistency of the impedance computation tools should be verified. Secondly, the completeness of the impedance models should be ensured through different (and complementary) sets of bench and, if possible, beam-based measurements. Thirdly, impedance checks of any layout modification or new device installations should be performed. Finally, the impedance sources causing performance limitations should be identified and impedance optimization strategies implemented. The choice of the most appropriate strategy requires the knowledge of the knobs to manipulate the impedance. Simplified formulae where all the main dependencies are explicit or step by step simulations, which allow a deep understanding of the impedance mechanism, are very useful to define the optimization strategy.

## SPS FERRITE LOADED KICKERS

In this section the example of the SPS ferrite loaded kickers will be discussed to give an example of how a deep understanding of the impedance mechanism can be reached. A kicker is a special type of magnet designed to abruptly

deflect the beam off its previous trajectory, to inject the beam into a ring or extract it to a transfer line or to a beam dump. H. Tsutsui derived a field matching theory to obtain the longitudinal [1, 2] and transverse dipolar [3] impedance of a geometrical model made of two ferrite blocks inserted inside a metallic chamber (see Fig. 1), for an ultra-relativistic beam. The model for the ferrite permeability  $\mu$  as a function of frequency  $f$  can be obtained from a first order dispersion fit on measured data:

$$\mu = \mu_0 \cdot \mu_r = \mu_0 \left( 1 + \frac{\mu_i}{1 + jf2\pi\tau_u} \right) \quad (1)$$

where  $\mu_i$  and  $\tau_u$  are the parameters of the fit and  $\mu_0$  is the vacuum permeability. The ferrite dielectric properties are characterized by a complex permittivity  $\varepsilon$ :

$$\varepsilon = \varepsilon_0 \cdot \varepsilon_r = \varepsilon_0 \left( \varepsilon'_r - \frac{j\sigma_{el}}{2\pi f\varepsilon_0} \right) \quad (2)$$

where  $\sigma_{el}$  is the DC electrical conductivity of the ferrite,  $\varepsilon_0$  the vacuum permittivity and  $\varepsilon'_r$  the dielectric constant. Tsutsui's theoretical impedance calculations were compared to HFSS [4] simulations and subsequently to measurements of PS and SPS kickers in references [5–7]. In his paper [3], H. Tsutsui only derived the transverse dipolar impedances, while the quadrupolar part was first derived in [8]. The analytical calculations of the beam impedance using, for instance, the models of Tsutsui are unfortunately restricted to simplified geometrical models so that the equations can be solved analytically. We will gradually move from the simplified models to more realistic, and hence complicated, structures.

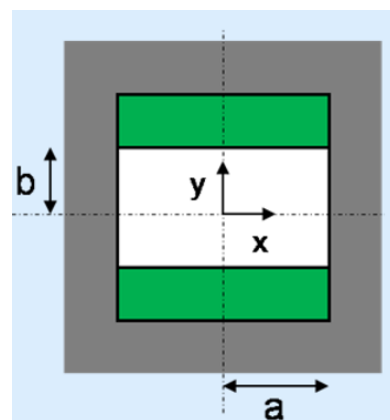


Figure 1: Geometrical kicker model described by Tsutsui: vacuum (white); 2 ferrite blocks (green) transversely surrounded by perfect electric conductor (gray).

\* carlo.zannini@cern.ch

### EM simulations of SPS kickers

First of all, CST Particle Studio Wakefield simulations [9] of the model of Fig. 1 have been performed [10, 11]. These simulations have been compared to the theoretical impedance obtained with the H. Tsutsui formalism for the longitudinal and the transverse impedances [12]. The very good agreement between the analytical model and the simulations makes the Wakefield solver of CST Particle Studio a reliable tool to simulate the impedance of dispersive materials such as ferrite. The Tsutsui model of Fig. 1, despite its simplicity, could explain both the "negative" total horizontal impedance observed in bench measurements [12] and the positive horizontal tune shift measured with beam in the SPS [6]. However, in this simple model several features of the kicker magnets have been neglected.

As a first step, the impedance of a C-Magnet kicker without the High Voltage (HV) conductor has been calculated analytically [13]. However, a device of finite length inserted in the vacuum tank and equipped with an inner conductor can support propagation of a Quasi-TEM mode when interacting with the beam. The device behaves as a transmission line formed by the vacuum tank and the inner conductor which are continued on the external cables and closed on the appropriate circuit terminations. This behaviour disappears as soon as we allow for 2-D geometries (infinite in the longitudinal direction) because the Quasi-TEM mode arises at the discontinuities. For this reason, if we want to consider the interaction of the beam with the Quasi-TEM mode, we must resort to a 3D C-Magnet model (see Fig. 2).

In the frame of an improvement of the kicker impedance model we performed a step by step simulation study starting from the simplest model and introducing one by one the new features that bring the model gradually closer to reality. This approach allows for a good understanding of the different contributions brought to the kicker impedance by the different aspects. First, the ferrite is assumed to be C-shaped and the whole finite length device is inserted in the vacuum tank and equipped with an inner conductor [14].

In order to further approach a more realistic model other aspects must be included: the cell longitudinal structure (also called segmentation), transitions between the ferrite blocks and the beam pipe, external coupling circuits, geometry outside of the ferrite yoke and shielings.

**Effect of the longitudinal segmentation** C-cores ferrites are sandwiched between HV capacitance plates. Plates connected to ground are interleaved between the HV plates: the HV and ground plates form a capacitor to ground. One C-core, together with its HV and ground capacitance plates, is named a cell [15]. The impact of segmentation in cells on the beam coupling impedance has been studied in detail. In the frequency range of interest (from few tens of MHz up to few GHz) for the SPS impedance model, the segmentation is found to have a significant effect only on the injection kickers (MKPs). For the other kickers the effect of the segmentation is negligible since the wavelength is sufficiently

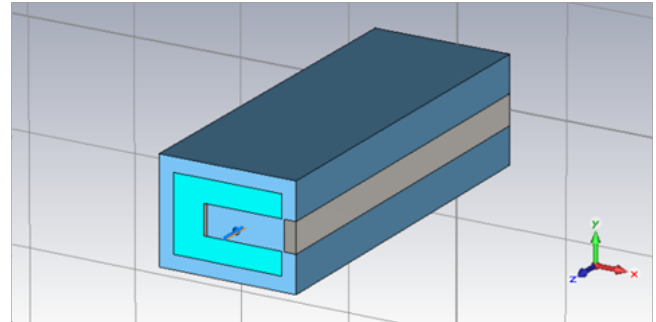


Figure 2: Geometric models for impedance calculation: ferrite in turquoise, perfect electric conductor in gray and vacuum in blue.

small compared to the cell length.

The 3-D simulation model of the SPS injection kicker (MKP-L) is illustrated in Fig. 3. The kicker module is divided into 22 cells, each of 26 mm length. The effect of the longitudinal segmentation on the beam coupling impedance is expected to be significant since the wavelength has been estimated to be comparable with the cell length [16]. As an example, in order to show the effect of such a dense longitudinal segmentation, we compared in Fig. 4 the longitudinal impedance with and without segmentation. The effect of segmentation is visible below 1 GHz, where a significant enhancement of the impedance is observed.

MKP-L is presently the bottleneck for the CERN-SPS beam induced heating. A design solution to optimize the impedance with serigraphy is available [17] and the prototype validation is ongoing. The impedance models of the segmented SPS injection and extraction kickers have been successfully benchmarked with bench measurements [16, 17].

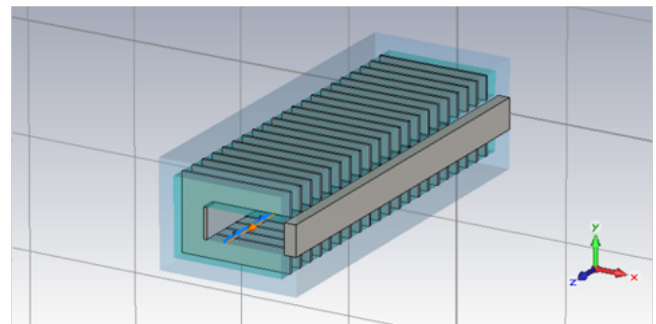


Figure 3: Advanced model of the MKP kicker module.

**SPS extraction kicker: effect of the serigraphy** Due to heating issues [18] the original design of these kickers was modified [19]. Interleaved fingers were printed by serigraphy directly on the ferrite. The beam induced heating is directly related to the beam power loss through the real part of the longitudinal impedance. The serigraphy results in a strong reduction of the real part of the longitudinal impedance over a broad frequency range [7, 19, 20]. The broad-band peak shifts from  $\approx 600$  MHz to  $\approx 3.3$  GHz

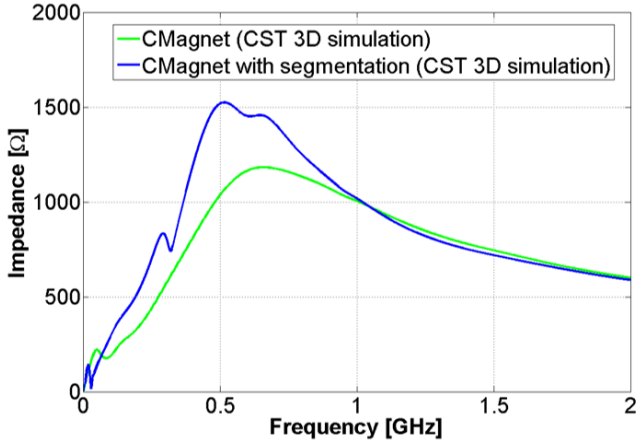


Figure 4: Comparing the longitudinal impedance for the MKP-L with and without segmentation.

and at the same time the serigraphy introduces a clear resonance at 44 MHz [21]. This resonance was studied in detail and was identified to be a quarter wavelength resonance on the silver fingers [16, 21]. To minimize the impact of this resonance on the beam induced heating the finger length could be optimized to shift the resonance frequency as far as possible from the beam spectrum lines. This required shortening the serigraphy length by 20 mm [22]. The solution has been implemented and experimentally validated during SPS scrubbing runs [23]. This solution has given an additional 40% margin in the SPS bunch intensity, which is crucial for the HL-LHC beams.

The example of the SPS ferrite loaded kickers shows the importance of a step by step approach from simplified to complex models involving 3D electromagnetic simulations and analytical calculations to reach a very good understanding of the impedance mechanism and to find the best design solution for impedance optimization.

## IMPEDANCE REDUCTION IS NOT ALWAYS BENEFICIAL

Impedance optimization is an extremely complex task that requires a global view of the impedance induced effects and of the machine criticalities. The best option is not always the one with the lowest impedance. For example, while reducing the longitudinal impedance is beneficial in terms of beam induced heating, the reduction of the transverse impedance could be detrimental for beam stability. To illustrate this concept, the transverse impedance model of the SPS extraction kickers in their original design has been taken into consideration, as well as the same impedance reduced by a factor of 5 (see Fig. 5).

The effect on beam dynamics can be qualitatively assessed using the concept of effective impedance. For bunched beams the impedance is sampled at an infinite number of discrete frequencies given by the mode spectrum. An "effective coupling impedance" can then be defined as the sum over

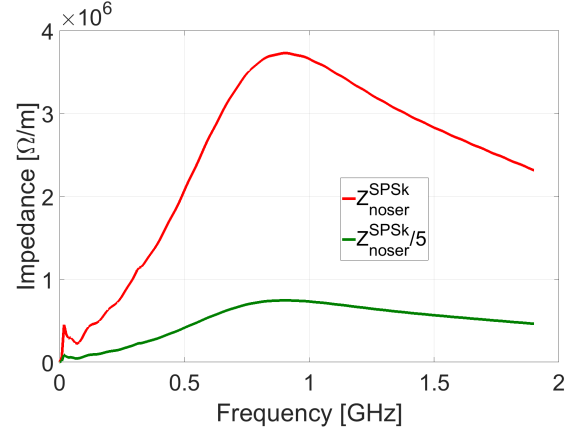


Figure 5: Impedance model of the SPS kickers without serigraphy and same impedance reduced by a factor of 5.

the product of the coupling impedance and the normalized spectral density. The "effective coupling impedance" is required for the calculation of both longitudinal and transverse complex tune shifts of bunched beam and can be defined in the transverse plane as [24–26]:

$$(Z_{\perp})_{\text{eff}} = \frac{\sum_{p=-\infty}^{p=\infty} Z_{\perp}(\omega' + \omega_{\beta}) h_l(\omega' + \omega_{\beta} - \omega_{\xi})}{\sum_{p=-\infty}^{p=\infty} h_l(\omega' + \omega_{\beta} - \omega_{\xi})} \quad (3)$$

Here  $h_l(\omega)$  is the power spectral density,  $\omega_{\beta}$  is the betatron angular frequency,  $\omega_{\xi}$  is the chromaticity frequency shift and  $\omega' = \omega_0 p + l\omega_s$  where  $\omega_0$  is the revolution angular frequency,  $\omega_s$  is the synchrotron frequency and  $l$  determines the type of oscillations (the case  $l = 0$  describes the single-bunch head-tail instabilities). For a Gaussian bunch,  $h_l(\omega)$  can be written as:

$$h_l(\omega) = \left(\frac{\omega\sigma_z}{c}\right)^{2l} e^{-\frac{\omega^2\sigma_z^2}{c^2}} \quad (4)$$

where  $\sigma_z$  is the standard deviation of the Gaussian bunch profile (root mean square (RMS) bunch-length) and  $c$  is the speed of light in vacuum. The real and the imaginary parts of the "effective impedance" give the growth rate and the frequency shift of the mode under consideration respectively. [26–29].

If the real part of  $(Z_{\perp})_{\text{eff}}$  is negative, the beam can become unstable. The real part of the transverse impedance is an odd function of frequency. Therefore, for the mode  $l = 0$ , simply assuming that the impedance is positive for positive frequencies leads to the conclusion that this mode would be stable for positive spectral shift and unstable for negative spectral shift (see Fig. 6). The situation is different if we consider higher mode numbers. For a given chromatic shift the sign of the effective impedance depends on the impedance type. Therefore, no general rule for stability criteria can be given for these modes. Figure 7 for example shows an illustrative view of the mode  $l = 1$  together with a capacitive

impedance (decreasing with frequency) and an inductive impedance (increasing with frequency). For the resistive wall impedance (capacitive impedance) and for  $\xi < |\xi_{max}|$  ( $\xi_{max}$  is defined as the chromaticity value at which the first sign inversion of the growth rate occurs) the mode  $l = 1$  is destabilizing for positive chromaticity and stabilizing for negative chromaticity, the situation is exactly reversed in the case of the impedance of ferrite loaded kickers (inductive impedance up to almost 1 GHz).

The overall effect of different impedance contributions depends on the weight of stabilizing and destabilizing effects. An inductive impedance has a stabilizing effect for mode  $l = 1$  and  $\xi > 0$ . Reducing this kind of impedance makes the situation worse. Therefore, coming back to the example of Fig. 5 reducing the impedance by a factor of 5 also reduces the stabilizing effect of this impedance for positive chromaticity (see Fig. 8) making the overall situation in terms of beam stability worse (see Fig. 9). The results obtained have been also confirmed with the DELPHI Vlasov solver [30] (see Fig. 10).

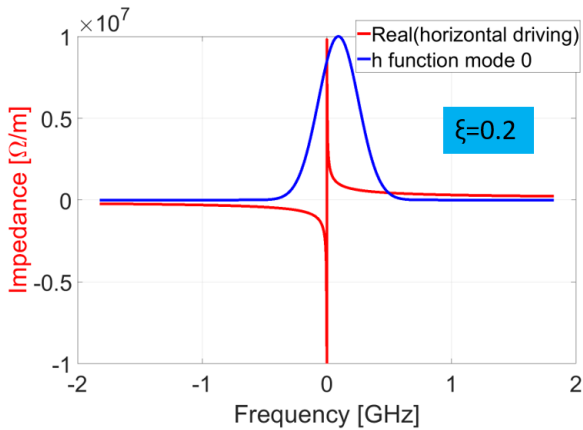


Figure 6: SPS wall impedance model (red) and power spectral density for the mode  $l = 0$  in arbitrary units for a chromaticity  $\xi = 0.2$  (blue) at injection energy for the Q20 optics.

### IMPEDANCE DUE TO COUPLING WITH CABLES

As previously described, as a first step a ferrite loaded kicker can be modeled as two parallel plates of ferrite surrounded by perfect electric conductor, i.e. the Tsutsui model. This model is expected to be valid only above a certain frequency (when the Quasi-TEM mode has no effect because the penetration depth in the ferrite is small compared to the magnetic circuit length [13]). In 1979 Sacherer and Nassibian [31] calculated the TEM impedance contribution for longitudinal and dipolar horizontal impedances for the C-Magnet model. These calculations have been reviewed in Ref. [14] where all the impedance terms for the C-Magnet model have been calculated and successfully benchmarked with EM simulations. The total beam coupling impedance of the C-Magnet kicker (longitudinal, constant [32], driving

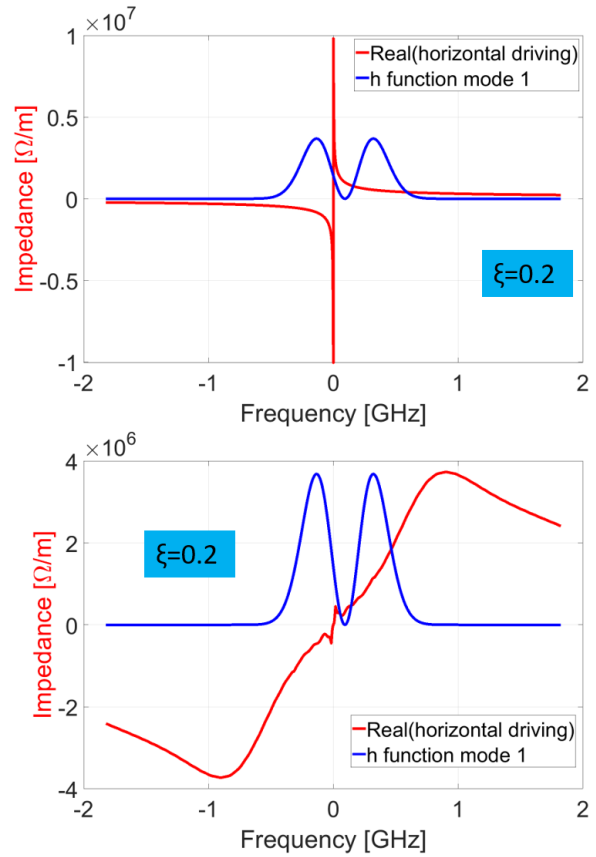


Figure 7: Power spectral density for the mode  $l = 1$  in arbitrary units for a chromaticity  $\xi = 0.2$  (blue) together with the SPS wall impedance model (top) and the SPS kickers without serigraphy (bottom) at injection energy for the Q20 optics.

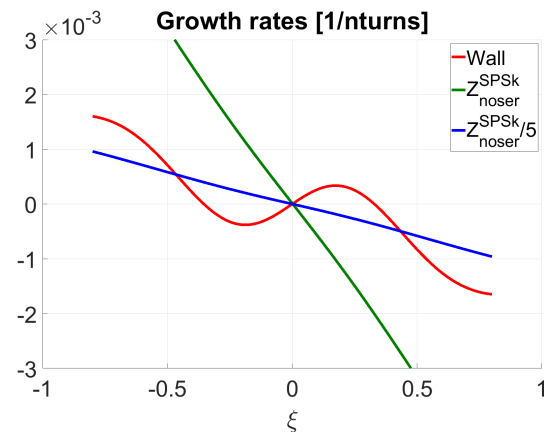


Figure 8: Horizontal growth rates versus chromaticity of the mode  $l = 1$  for the SPS resistive wall impedance (red), the SPS kickers without serigraphy (green), and the SPS kickers impedance without serigraphy reduced by a factor of 5 (blue).

and detuning) of Fig. 2 is calculated using the superposition of the effects. Indeed for these devices the impedance

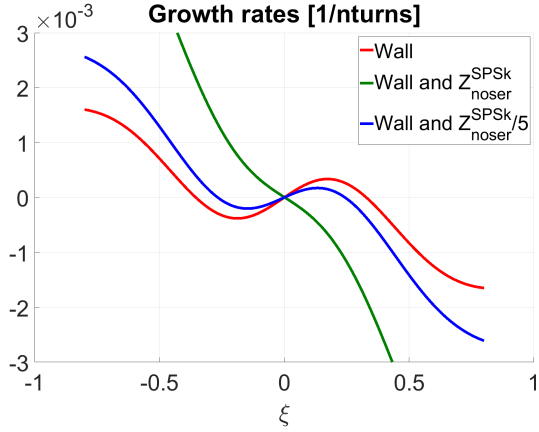


Figure 9: Horizontal growth rates versus chromaticity of the mode  $l = 1$  for the SPS resistive wall impedance (red), the SPS wall impedance plus the SPS kickers without serigraphy (green), and the SPS wall impedance plus the SPS kickers impedance without serigraphy reduced by a factor of 5 (blue).

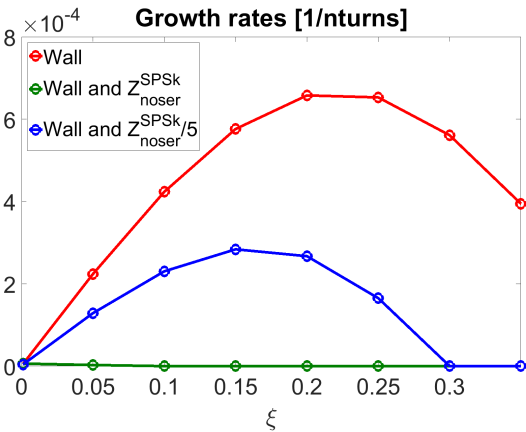


Figure 10: Horizontal growth rates versus chromaticity of the most unstable mode (DELPHI calculations) for the SPS resistive wall impedance (red), the SPS wall impedance plus the SPS kickers without serigraphy (green), and the SPS wall impedance plus the SPS kickers impedance without serigraphy reduced by a factor 5 (blue).

arises from core losses and coupling to the external circuits through the kicker supply line [14, 16]. Figure 11 shows the equivalent circuit of the model. More details about the model can be found in Ref. [14, 16]. The model allows to calculate the impedance due to coupling with the kicker circuit. The kicker circuit is represented as the equivalent impedance  $Z_g$ . Therefore, the model can consider whatever kind of circuit as long as this can be represented with an equivalent impedance.

The impedance due to coupling with the external circuits can also be directly simulated with the Wakefield solver of CST Particle Studio using the simulation method described in Ref. [16].

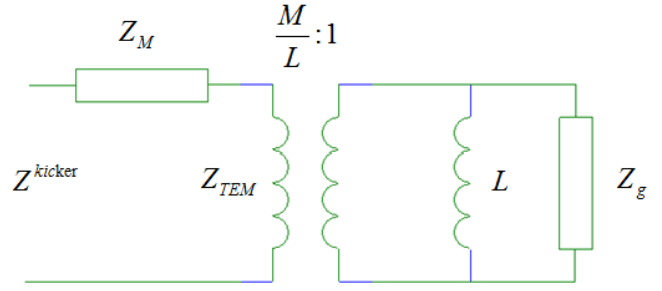


Figure 11: Circuit model of the kicker including cables.  $Z_{TEM}$  is the impedance contribution due to the coupling with the external circuits,  $Z_M$  the impedance contribution due to core losses,  $L$  is the inductance of the magnet circuit,  $Z_g$  the external impedance including cables and  $M$  the mutual inductance of the magnet.

### Example of the PSB extraction kicker

The ejection kicker of the PSB is analyzed as an example of interest for the model. A schematic of the kicker circuit is shown in Fig. 12. The external impedance including cables  $Z_g$  is calculated solving the circuit and transporting the loaded impedance at the termination over the cable length using the transmission line theory. Figure 13 shows the dipolar horizontal impedance of the ejection kicker (EK) of the PSB calculated using Eq. 2.58 of Ref. [16] with  $Z_g$  obtained solving the circuit of Fig. 12. The frequency pattern of the resonances depends on the single-way delays and termination of the kicker circuit. The very low attenuation constant of the cables makes these resonances narrow with a Q value of about 100 and a shunt impedance in the order of  $M\Omega/m$ . The first resonance appears at 1.72 MHz. The frequency values found in the model mainly depend on cable length and properties. The height and width of the peaks depend on the cable attenuation that is in the order of few  $mdB/m$  for the PSB cables. Concerning this point it is worth noting that the impedance of the resonances is inversely proportional to the attenuation. Figure 14 shows the impedance of the PSB extraction kicker assuming different cables attenuation. Therefore, decreasing cable attenuation the growth rate of the instability driven by the mode will also increase while the tune band at which the instability is driven will be narrowed due to the higher quality factor of the resonance.

The impedance of Figure 13, previously suspected in [16], was proven to be responsible for the head-tail horizontal instability observed in the PSB when the feedback system is off [33]. Once the source of the PSB horizontal instability was confirmed to be the impedance of the extraction kicker due to coupling with the external circuits, different design solutions have been investigated for impedance optimization [33]. The more promising impedance mitigation solution for the PSB extraction kicker which is presently under study is to insert a saturating inductor between the kicker module and the coaxial cables. This is expected to shift the first resonance to significantly lower frequency (see

Fig. 15). With this circuit modification a stable scenario is expected below half integer tune (see Fig. 16 and [33]). The example of the PSB extraction kicker highlights that the impedance from unmatched terminations of one single device can lead to violent beam instability. Therefore, a reliable model for the estimation of the impedance due to cable termination effects is crucial.

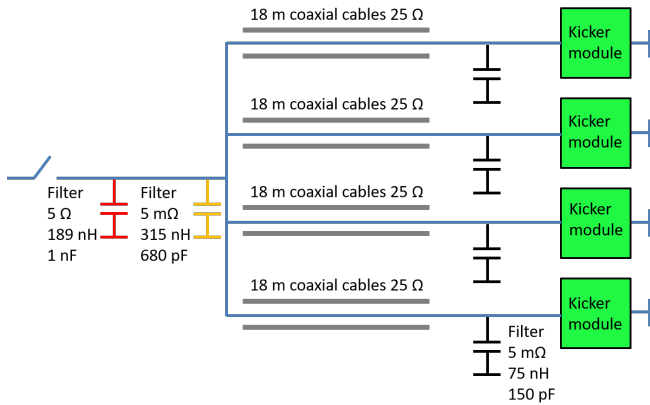


Figure 12: Schematic of the PSB extraction kicker circuit.

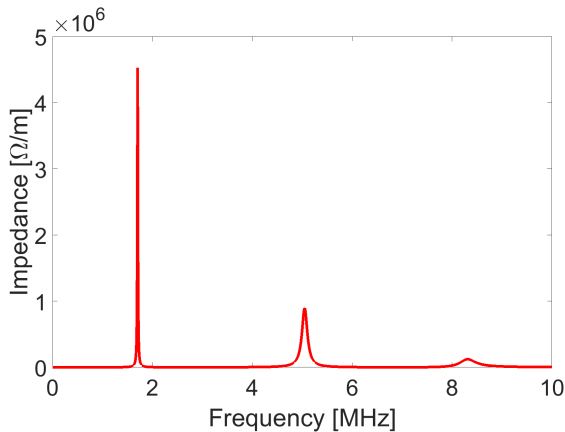


Figure 13: Real part of the driving horizontal impedance of the PSB extraction kicker due to the coupling with the circuit of Fig. 12.

## POTENTIAL OF METAMATERIALS FOR IMPEDANCE MITIGATION

Metamaterials or, more in detail, composite materials with negative values of either relative permittivity or relative permeability have been intensively studied in the last decades [34]. Concerning metamaterials insertions for beam-coupling impedance mitigation, their effect has been first addressed in [35] for resistive-wall beam-coupling impedance reduction. The effect of metamaterial insertions on beam-coupling impedance has been studied theoretically by means of a transmission-line model [16, 36]. Overall, the observed results demonstrate a remarkable influence on the resistive-wall beam-coupling impedance, which can lead to the identi-

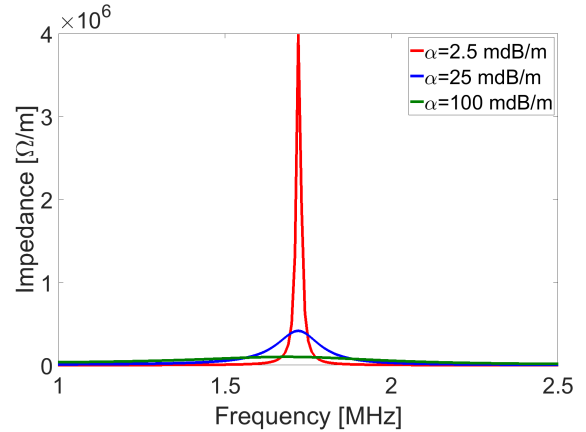


Figure 14: First resonance of the real part of the driving horizontal impedance of the PSB extraction kicker due to the coupling with the circuit of Fig. 12 for different cables attenuation.

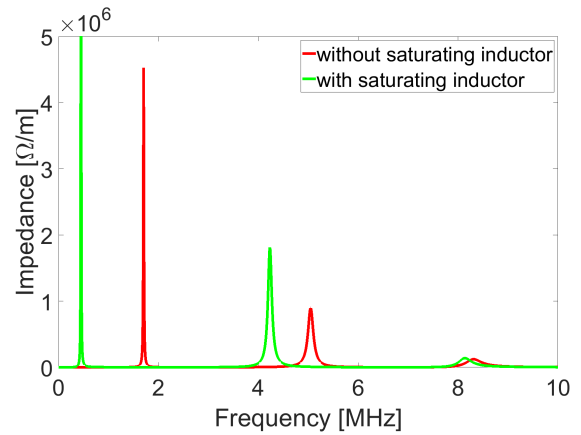


Figure 15: Real part of the driving horizontal impedance of the PSB extraction kicker due to the coupling with the circuit of Fig. 12 with and without saturating inductor between kicker module and coaxial cables.

fication of theoretical design rules for impedance mitigation, exploiting the different degrees of freedom: the type of material (epsilon negative (ENG) or mu negative (MNG)), its values of constitutive parameters, its thickness and its length. Therefore, a proper engineering of such insertions can be performed, with the aim of substantially reducing the resistive-wall impedance of a beam line.

As a proof of principle, experimental measurements were performed with splitting ring resonators (SRR) metamaterials. The measurements discussed and presented in [37] have been performed by evaluating the quality factor  $Q$  of several resonances in a cavity. The cavity has been obtained using a straight section of a rectangular waveguide WR284, enclosing it between two metallic plates and inserting a tiny antenna on one side, in order to excite the modes. Measurements have been performed with and without metamaterial insertions (two SRR stripes on the cavity walls, as depicted in Fig. 5 of Ref. [37]). The resonance frequencies on the  $S_{11}$

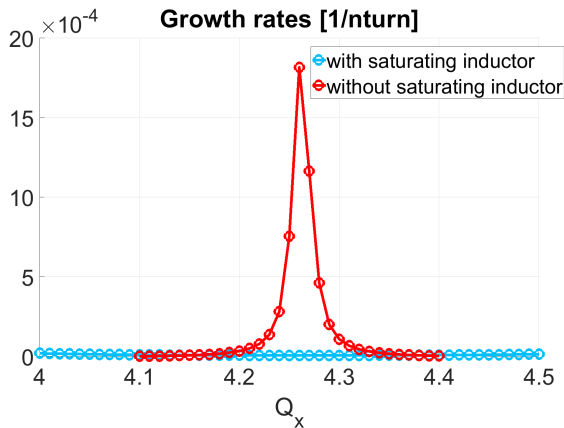


Figure 16: Horizontal growth rates versus betatron tune of the PSB due to the coupling with the circuit of Fig. 12 with and without saturating inductor between kicker module and coaxial cables.

spectra have been identified and the corresponding unloaded Q factors have been measured using a Vector Network Analyzer (VNA) and post-processing techniques.

The unloaded quality factor of a resonance associated to an empty waveguide section is related solely to the losses on the conductive walls. Such losses are due to the surface impedance of the walls, which depends on the material conductivity and frequency. The quality factor is inversely proportional to the surface resistance. Therefore, to interpret the results coming from the measurements, one should note that an increase of the unloaded quality factor testifies a proportional decrease of the resistive-wall impedance (caused by a decrease of the surface impedance). The measurement results of Fig.6 of Ref. [37] show that at about 2.9 GHz the measured unloaded Q is significantly higher in the case of metamaterial presence, meaning a decrease of an order of magnitude of the surface impedance. This demonstrates the potential of metamaterials to approach the equivalent behaviour of a perfect electrical conductive wall. The other peaks instead show little or no variation when the SRRs are put in the waveguide. This is expected since both material properties and the condition to get the equivalent behaviour of a perfect electric conductor are frequency dependent [37]. The possibility of using metamaterials to approach the behaviour of a perfect electric conductor could lead to the fascinating scenario of developing superconductive like cavities at ambient temperature and lossless guiding structures.

## CONCLUSION

A deep understanding of all the impedance induced effects is needed to make the best choice in terms of impedance optimization considering both local effects (direct effect on the device) and global effects (interplay between the different impedances). Impedance optimization is a very challenging task due to the several concurrent induced effects. As an example, it has been shown that impedance reduction, though desirable for equipment heating mitigation, can also

be detrimental in terms of beam stability. This also means that it could be considered to introduce ad hoc impedances to have beneficial effects on beam stability.

## REFERENCES

- [1] H. Tsutsui, "Some Simplified Models of Ferrite Kicker Magnet for Calculation of Longitudinal Coupling Impedance," *CERN-SL-2000-004-AP*, January 2000.
- [2] H. Tsutsui, "Longitudinal impedances of some simplified ferrite kicker magnet models," *CERN-SL-2000-050-AP*, June 2000.
- [3] H. Tsutsui and L. Vos, "Transverse Coupling Impedance of a Simplified Ferrite Kicker Magnet Model," *LHC-PROJECT-NOTE-234*, September 2000.
- [4] <https://www.ansys.com/products/electronics/ansys-hfss>.
- [5] F. Caspers, A. Mostacci, and H. Tsutsui, "Impedance Evaluation of the SPS MKE Kicker with Transition Pieces between Tank and Kicker Module," *CERN-SL-2000-071-AP*, October 2000.
- [6] E. Métral, F. Caspers, M. Giovannozzi, A. Grudiev, T. Kroyer, and L. Sermeus, "Kicker impedance measurements for the future multiturn extraction of the CERN Proton Synchrotron," *CERN-AB-2006-051*, July 2006.
- [7] M. J. Barnes, F. Caspers, T. Kroyer, E. Métral, F. Roncarolo, and B. Salvant, "Measurement of the longitudinal and transverse impedance of kicker magnets using the coaxial wire method," *CERN-ATS-2009-018*, July 2009.
- [8] B. Salvant, N. Mounet, C. Zannini, E. Métral, and G. Rumolo, "Quadrupolar Transverse Impedance of Simple Models of Kickers," *CERN-ATS-2010-076*, June 2010.
- [9] "<http://www.cst.com/>,"
- [10] C. Zannini and B. Salvant, "Update on the impedance of the SPS kicker," Presented at the SPS impedance meeting (<https://impedance.web.cern.ch>), October 2009.
- [11] C. Zannini, "Simulations of the SPS kickers with CST Particle Studio," Presented at the SPS impedance meeting (<https://impedance.web.cern.ch>), August 2009.
- [12] C. Zannini, N. Mounet, B. Salvant, E. Métral, and G. Rumolo, "Electromagnetic simulations of simple models of ferrite loaded kickers," *CERN-ATS-2010-098*, June 2010.
- [13] C. Zannini, V. G. Vaccaro, E. Métral, G. Rumolo, and B. Salvant, "Electromagnetic modeling of C-shaped ferrite loaded kickers," *CERN-ATS-2011-103*, September 2011.
- [14] C. Zannini, G. Rumolo, and V. G. Vaccaro, "Effect of the TEM Mode on the Kicker Impedance," *CERN-ATS-2012-134*, May 2012.
- [15] M. Barnes, "Kicker systems," *CERN Yellow Rep. School Proc.*, vol. 5, p. 229. 55 p, 2018.
- [16] C. Zannini, *Electromagnetic Simulation of CERN accelerator components and experimental applications*. PhD thesis, Lausanne, EPFL, Switzerland, 2013. CERN-THESIS-2013-076.
- [17] M. S. Beck, "Simulation, measurement and mitigation of the beam induced power loss in the SPS injection kickers," Master's thesis, KIT, Germany, 2015. CERN-THESIS-2015-374.

- [18] M. Timmins, “SPS extraction kicker magnet: thermal analysis,” *TS-Note-2004-016*, July 2004.
- [19] T. Kroyer, F. Caspers, and E. Gaxiola, “Longitudinal and Transverse Wire Measurements for the Evaluation of Impedance Reduction Measures on the MKE Extraction Kickers,” *CERN-AB-Note-2007-028*, July 2007.
- [20] E. Gaxiola, J. Bertin, F. Caspers, L. Ducimetière, and T. Kroyer, “Experience with Kicker Beam Coupling Reduction Techniques,” *CERN-AB-2005-024*, June 2005.
- [21] C. Zannini and G. Rumolo, “EM Simulations in Beam Coupling Impedance Studies: Some Examples of Application,” EuCARD-CON-2012-016 (<http://cds.cern.ch/record/1498077>), ICAP12, 2012.
- [22] C. Zannini, “Multiphysics Simulations of Impedance Effects in Accelerators,” *CERN Yellow Rep. Conf. Proc.*, vol. 1, pp. 141–144, 2018.
- [23] M. Barnes, M. Beck, H. Day, L. Ducimetière, E. Garcia-Tabares Valdivieso, B. Goddard, H. Neupert, A. Romano, L. Vega Cid, W. Weterings, and C. Zannini, “Upgrading the SPS Fast Extraction Kicker Systems for HL-LHC,” *CERN-ACC-2017-217*, 2017.
- [24] B. W. Zotter, “The effective coupling impedance for instabilities of Gaussian bunches,” *CERN-ISR-TH-80-03*, 1980.
- [25] B. W. Zotter, “The effective coupling impedance for bunched beam instabilities,” *CERN-ISR-TH-78-16*, 1978.
- [26] A. W. Chao, *Physics of collective beam instabilities in high energy accelerators*. New York: Wiley, 1993.
- [27] B. W. Zotter, “Collective effects: General description,” *CERN-85-19-V-2*, pp. 415–431, 1984.
- [28] J. L. Laclare, “Introduction to coherent instabilities: Coasting beam case,” *CERN-85-19-V-2*, pp. 377–414, 1985.
- [29] J. L. Laclare, “Bunched beam coherent instabilities,” *CERN-87-03-V-1*, pp. 264–326, 1987.
- [30] N. Mounet, “Vlasov Solvers and Macroparticle Simulations,” *CERN Yellow Rep. Conf. Proc.*, vol. 1, pp. 77–85, 2018.
- [31] G. Nassibian and F. J. Sacherer, “Methods for measuring transverse coupling impedances in circular accelerators,” *Nucl. Instrum. Methods*, vol. 159, no. 1, pp. 21–27, 1979.
- [32] C. Zannini, K. Li, and G. Rumolo, “Effects of an Asymmetric Chamber on the Beam Coupling Impedance,” *CERN-ATS-2012-081*, May 2012.
- [33] E. Koukovini-Platia, M. J. Barnes, H. Bartosik, G. Rumolo, L. Sermeus, and C. Zannini, “Source of horizontal instability at the CERN Proton Synchrotron Booster,” *Phys. Rev. Accel. Beams*, vol. 22, no. 12, 2020.
- [34] N. Engheta and R. Ziolkowski, *Metamaterials: Physics and Engineering Explorations*. John Wiley & Sons, Inc., 9 2006.
- [35] A. Danisi, C. Zannini, A. Masi, R. Losito, and B. Salvant, “Theoretical Analysis of Metamaterial Insertions for Resistive-Wall Beam-Coupling Impedance Reduction,” *CERN-ACC-2014-0191*, 2014.
- [36] C. Zannini, “TLwall: transmission line model for wall impedance calculation,” Presented at the CERN HSC section meeting (<https://indico.cern.ch/event/795854/>), February 2019.
- [37] A. Danisi, C. Zannini, R. Losito, and A. Masi, “Metamaterial insertions for resistive-wall beam-coupling impedance reduction,” *arXiv:1910.02246*, 2019.